ACS APPLIED MATERIALS & INTERFACES

www.acsami.org

Research Article

Microinjectors for Controlled Cross-Barrier Drug Delivery in the Gastrointestinal Tract

Joshua A. Levy, Michael A. Straker, Justin M. Stine, Jude A. C. Stephen, and Reza Ghodssi*

Cite This: ACS Appl. Mater. Interfaces 2025, 17, 36420−36432

Read Online

ACCESS | Metrics & More | Article Recommendations | Supporting Information

ABSTRACT: The gastrointestinal tract is a desirable target for drug delivery because it acts as a gateway to the body through intestinal uptake mechanisms and because it is preferred by patients leading to better outcomes. While ingestible devices have been developed to enable delivery of drugs at specific locations in the intestinal tract using various methods, one undeveloped area of gastrointestinal drug delivery is controlled release from devices operating in the intestinal tract. In this work, a versatile combination of semiresident injection technologies has been developed to allow tunable drug delivery of >5 μL with half-lives between 4 s and 118 days. The injectors rely on a previously developed ingestible actuation technology to deploy into the intestinal tissue and prompt dosing across the mucosal barrier. The injectors are composed of a hybrid 3D-printed reservoir and microneedle structure with variable material and geometric properties to enable tailored dosing. The demonstrated technology provides a framework for higher-level control over drug delivery using advanced fabrication techniques to achieve versatile and advantageous structural properties.

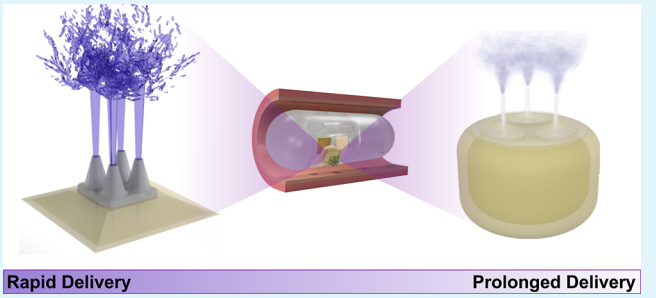

KEYWORDS: *gastrointestinal drug delivery, direct laser writing, 3D printing, ingestible device, hybrid fabrication, diffusion control*

INTRODUCTION

Oral delivery of drugs is the preferred therapeutic route by patients, leading to greater adherence to treatment protocols and overall health outcomes when available.[1,2] The gastrointestinal (GI) tract is primarily responsible for absorbing nutrients through the embedded vasculature and lymphatic capillaries in the intestinal mucosa, providing opportunities for targeted delivery to these physiological systems.[3] For example, intestinal delivery could enable minimally invasive drug release into systemic circulation or direct targeting of the lymphatic system.[4−7] However, delivered drugs are often required to pass through the intestinal mucosal barrier, where the combination of mucus and the epithelium resists absorption, especially drugs with large hydrodynamic size and charge, lowering bioavailability and increasing dosage requirements.[8,9] Moreover, the GI tract is a harsh environment with variable pH (1.5−7.4) and composition that can degrade exposed drugs throughout transit.[10−12] Consequently, technologies to transport and facilitate controlled release of drugs at points of interest in the intestinal tract would be coveted for their ability to enable oral delivery of traditional parenteral drugs.

Various techniques have been explored in academic literature to facilitate cross-barrier drug delivery in the GI tract.[13−16] A developing approach uses nanoparticle drug carriers for transcellular transport across the intestinal mucosal barrier.[7,17−22] At its current stage, this approach is challenging because, in most applications, the rate of transcellular transport is insufficient.[23] Moreover, while targeting of diseased areas using such technologies is an active area of research, no successful clinical examples exist.[24] An alternative approach evaluated by device researchers is the application of passive ingestible devices for mechanical perturbation of the mucosal barrier.[15,25,26] In this approach, microscale or millimeter-scale needles are used to pierce the mucosal barrier and release the drug.[27−29] This is most commonly in the form of dissolving microneedles; however, hollow microneedles have been explored.[30] For example, Abramson et al. have developed a self-orienting mm-scale applicator (SOMA) that injects a millineedle into the stomach wall for systemic drug release.[29]

Another noteworthy opportunity for gastrointestinal drug delivery involves localized drug delivery to release locally active drugs at sites of affliction or advantageous regions to improve efficacy (e.g., high absorption).[31,32] Localized drug delivery can be achieved through several techniques, ranging from passive dissolution-guided approaches to actively triggered robotic pills.[33] The simplest and most widely utilized form of localized delivery uses passive pill coatings or casings that dissolve in

Received: March 13, 2025
Revised: June 5, 2025
Accepted: June 8, 2025
Published: June 13, 2025

https://doi.org/10.1021/acsami.5c05183
ACS Appl. Mater. Interfaces 2025, 17, 36420−36432

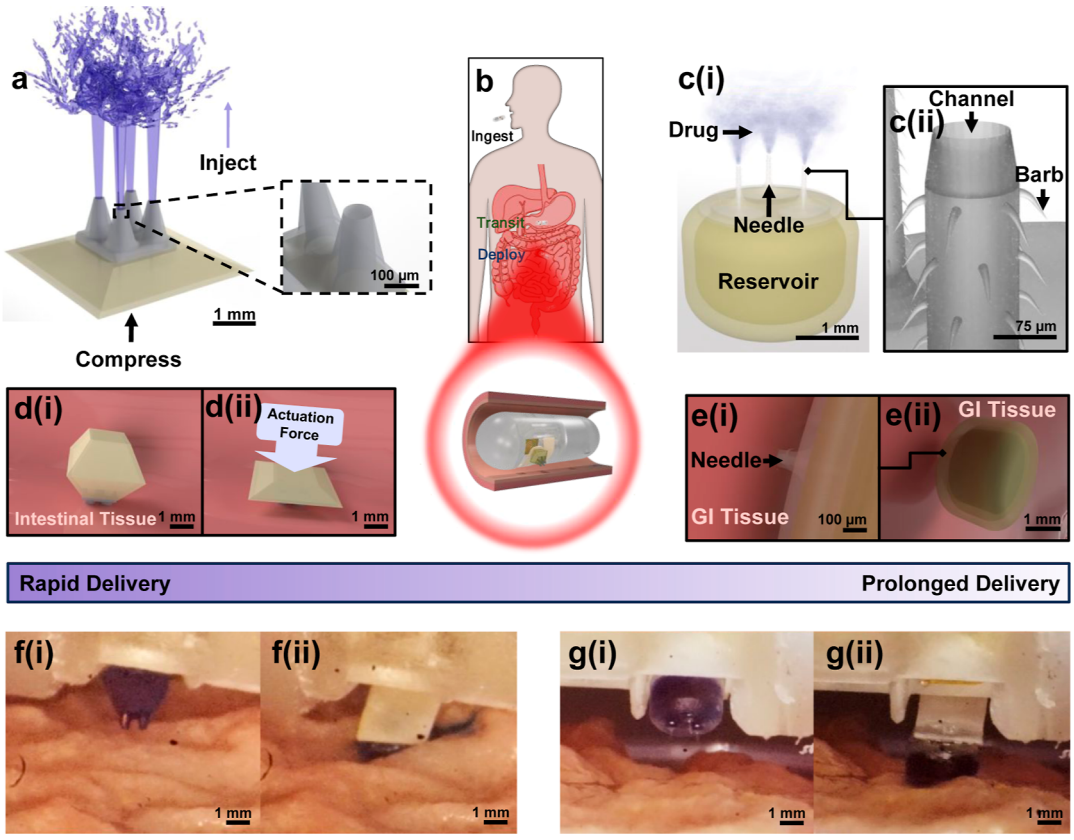

Figure 1. Overview of the versatile injection system. (a) The flexible injection system uses actuation force to achieve rapid injection into intestinal tissue. (b) Overview of the device application including ingestion, transit through the upper GI tract, and deployment at the site of need. (c) The rigid injector that relies on diffusion for control over prolonged drug delivery and barbed anchoring microneedles for anchoring in the intestinal tissue. (d) Sequential operation of the flexible injector where (d(i)) the injector microneedles first enter the intestinal tissue and then (d(ii)) the injector is compressed by an actuator force for injection. (e) Prolonged operation of the rigid injector where (e(i)) the needles anchor in the intestinal tissue and (e(ii)) diffusively release the drug into the surrounding tissue for prolonged localized treatment. (f(i,ii)) Deployment of the flexible injector into ex vivo porcine intestinal tissue. (g(i,ii)) Deployment of the diffusional injector into ex vivo porcine intestinal tissue.

specific pH-graded regions of the GI tract (e.g., stomach, small intestine) dependent on their use case.[1,11,34] Passive ingestible injection devices can also use these pH-specific materials as a trigger for region-specific drug delivery; however, this regional level of control is only useful in specific applications.[28,35] Actively controlled ingestible capsules with embedded sensors offer an alternative approach to control the specific site of drug release.[36] For example, devices like IntelliCap and others were developed to release liquid drug on command from a reservoir.[37−47] While fluid release capsules are useful, mechanisms for deployment or actuation toward the intestinal wall are required to access beyond the intestinal mucosal barrier. Lee et al. have demonstrated drug-eluting microneedles deployed using a magnetically guided capsule system.[48,49] The greatest clinical drawback of this system is the requirement of complex external electromagnetic equipment for its operation. In prior work, Levy et al. addressed this challenge by developing an ingestible capsule that uses a simple magnetic switching mechanism to activate actuators for drug delivery, requiring only a hand-held magnet for remote deployment of dissolving microneedles.[50] The prior capsule contained a battery, magnetic switch, and heating element that released a cantilever to deploy out of the capsule toward the GI wall, applying a force to deliver microneedles to the intestinal tissue.[50] In the prior work, a dissolving microneedle array was used as a drug storage element during the demonstration of actuator deployment.[50] However, the dissolving microneedles do not offer extensive versatility in the delivery time frame, depth, and location, evidencing a need for more control at the drug packaging level.

In this work, we develop a versatile microinjection technology for localized and controlled GI drug delivery from actuator-embedded ingestible capsules (Figure 1). The drug injectors are fabricated by a hybrid 3D-printing process merging mesoscale liquid crystal display (LCD) vat photopolymerization (VPP) 3D printing of drug reservoirs with direct laser writing (DLW) of hollow microneedles directly on the reservoirs for transport of drugs through the mucosal barrier and into the tissue. The microinjectors enable controlled loading volume, delivery time frame, and delivery location via changes in the reservoir material and needle geometry. Reservoirs fabricated with rigid material rely on diffusion out of the injector, while flexible reservoirs enable pumping by the applied actuator force, using the previously developed actuator capsule as a platform.[50,51] In both cases, the length and diameter of the hollow needle channel regulate the rate of release of fluid drug from the reservoir. This demonstration of versatility from such drug injectors is a major step forward for oral drug delivery, enabling controlled and localized dosing to improve treatment efficacy and outcomes.

https://doi.org/10.1021/acsami.5c05183
ACS Appl. Mater. Interfaces 2025, 17, 36420−36432

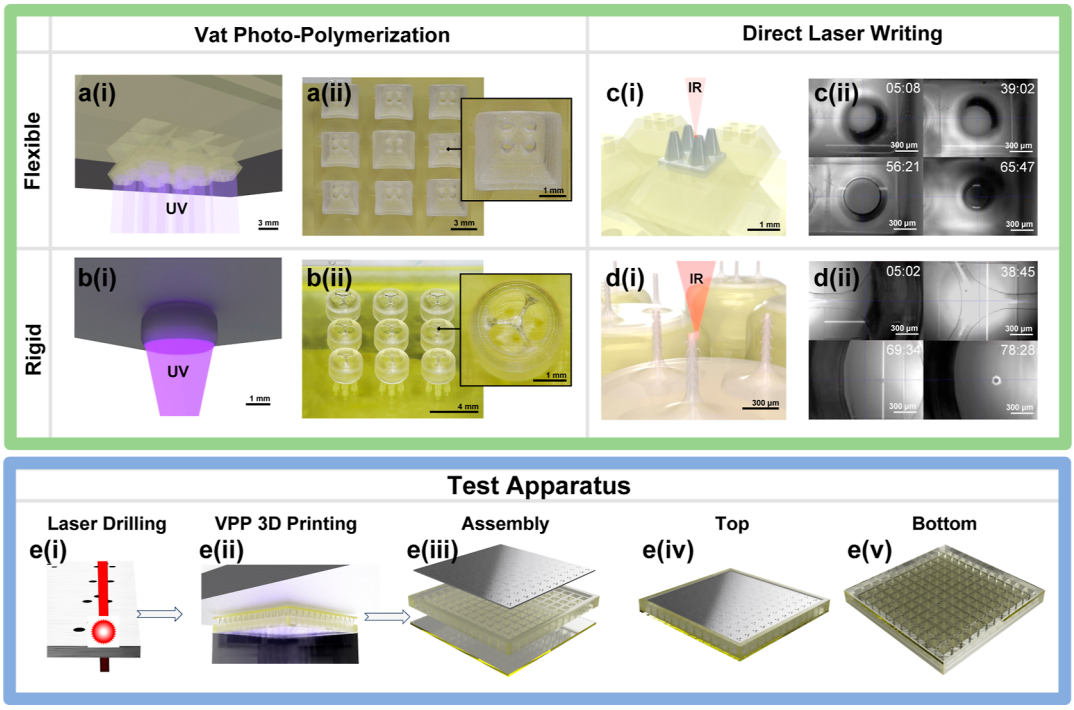

Figure 2. Hybrid fabrication of the injectors. (a(i),(ii)) Vat photopolymerization 3D printing of the flexible injector using a flexible biocompatible photoresin. (b(i),(ii)) Vat photopolymerization 3D printing of the flexible injector using a rigid biocompatible photoresin. (c(i),(ii)) Direct laser writing of the rigid conical hollow microneedles on top of the flexible reservoir using the Nanoscribe Photonic Professional GT+. (d(i),(ii)) Direct laser writing of the rigid barbed hollow microneedles on top of the rigid reservoir using the Nanoscribe Photonic Professional GT+. (e) Fabrication of the test apparatus for benchtop diffusional and flow analysis. The process involved (e(i)) laser drilling of channels in a 304 stainless steel plate, (e(ii)) VPP 3D printing of wells for drug loading, and (e(iii)) attachment of the channel plate to the 3D-printed wells. (e(iv),(v)) The fabricated diffusional test apparatus.

RESULTS AND DISCUSSION

Device Assembly and Operation. Drug injectors were fabricated using a hybrid process that combines vat photopolymerization (VPP) liquid crystal display (LCD) 3D printing of drug reservoirs with direct laser writing (DLW) of hollow microneedles. Reservoirs are printed on a support base in a 3 × 3 array for compatibility with the Nanoscribe DLW system (Figure 2a(i),b(ii)). Nanoscribe IPS is vacuum loaded into the reservoirs, and excess resin is placed atop the reservoirs before DLW. The microneedles are printed directly on the reservoirs with a rigid IP-Q photoresin (Figure 2c(i),d(ii)). Model drug solution is loaded into the reservoirs via vacuum loading, and delivery is driven and controlled by both diffusion and convection. In the case of the flexible injector, rapid convective delivery is achieved by compression of the reservoir; however, for the rigid injector, diffusion predominantly governs the release rate from the injector. The combination of methods enables control over a wide range of delivery profiles. Flexible injectors utilize a square shape to maximize loading volume, while rigid injectors are cylindrical to mitigate edge sharpness of the rigid structure. Dimensions of the injectors are shown in Figures S1 and S2. The hybrid 3D fabrication approach additionally permits features to be made over various scales and geometries, enabling large loading volumes with sharp and intricate needles to achieve advantageous characteristics, such as tissue anchoring. For evaluation of the injectors, a custom test apparatus was created using laser-drilled steel diffusion and flow channels and LCD 3D-printed diffusion and flow channels (Figure 2e(i),(v)).

The fabrication of the reservoirs, made in batches of 72 using LCD 3D printing, takes approximately 90 min. Fabrication of the needles, made with one injector at a time, takes approximately 66 min. Additional fabrication steps such as photopolymer development and drug loading are performed as batch processes. Thus, the current throughput bottleneck is in the fabrication of the needles using the Nanoscribe PPGT+. While DLW was employed to achieve rapid prototyping and design iteration, several approaches could be employed for fabrication of the injectors at scale, such as micromolding or projection microstereolithography (PμSL) that can achieve comparable feature sizes.[52] Future investigations into replicating injector characteristics using scalable processes will be conducted in the translation of this technology.

Computational Assessment of Flexible Injectors. The compression of the flexible injector is a product of the applied actuator force used to deploy the injector toward the gastrointestinal wall.[50] The actuator applies a force to the injector, which is converted to pressure inside the reservoir, prompting flow through the injection channels. The flow rate depends on the applied force, which can be tailored between 100 and 1500 mN by varying the cantilever actuator thickness. Compression of the injector body was evaluated using COMSOL Multiphysics finite element method (FEM) modeling to understand the required compression force for injection. A fixed constraint was applied to the bottom injector surface, and force was applied to the top surface of the injector. Figure 3a(i)−(iii) shows the total displacement of the injector when subjected to compressive forces between 50 and 250 mN. Figure 3b summarizes the linear relationship between force and displacement, resulting in an effective stiffness

https://doi.org/10.1021/acsami.5c05183
ACS Appl. Mater. Interfaces 2025, 17, 36420−36432

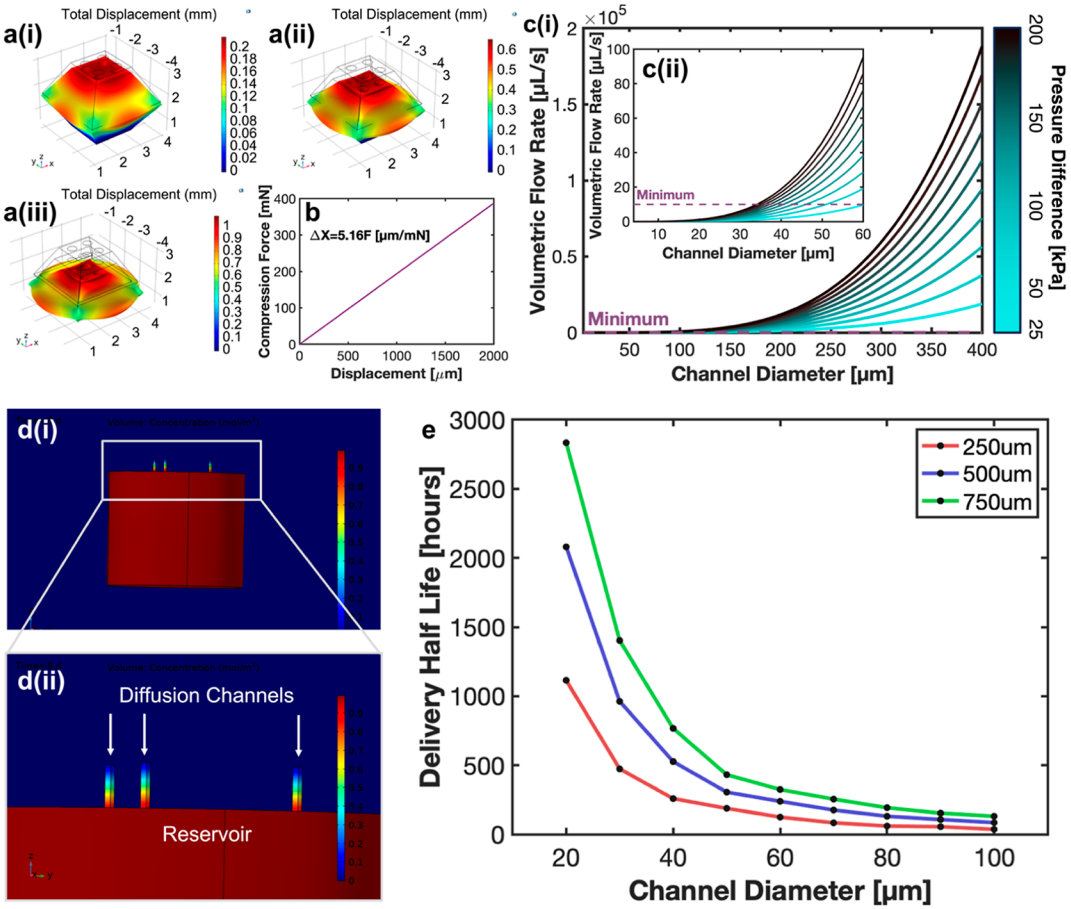

Figure 3. Computational assessment of the injector characteristics. (a) Compression of the flexible injector using COMSOL Multiphysics FEM software with forces of (a(i)) 50 mN, (a(ii)) 150 mN, and (a(iii)) 250 mN. (b) The relationship between compression force and displacement of the flexible injector top surface is linear with a proportionality constant of 5.16 μm·mN^{-1}. (c(i)) Computational evaluation of the flexible injector using the Hagen−Poiseuille equation shows (c(ii)) sufficient injection rates can be achieved with channel diameters as low as 60 μm at a pressure of 25 kPa. (d(i),(ii)) COMSOL Multiphysics model of diffusion of dilute species through a three-channel array into a large reservoir. The color gradient represents the concentration gradient where blue is low concentration and red is high concentration. (e) Diffusion half-life for a variety of channel diameters and lengths showing the predictability of the delivery time frame using the rigid drug injectors.

constant of 5.16 mN·μm^{-1}. Notably, contact constraints were not used in the interior of the reservoir, and the force required at higher compression values is expected to deviate from the linear behavior in Figure 3b. Nevertheless, this result validates that the flexible injectors can be readily compressed using achievable actuation forces of >500 mN demonstrated previously by Levy et al.[50] Moreover, the rigidity of the flexible reservoir below 50 mN is critical to enable microneedle penetration prior to compression of the reservoir. This sequential operation ensures optimal delivery efficiency by promoting drug release following insertion of the needles.

As the flexible injector does not utilize anchoring barbs, it is critical to achieve rapid emptying of the reservoir to avoid transient effects on actuation forces caused by peristaltic motion in the intestine. Given the supplementary actuation force beyond that required to compress the reservoir structure, the excess actuation force is expected to transfer pressure to the fluid inside the reservoir. Such pressure-induced flow can be modeled using the Hagen−Poiseuille equation, which describes the relationship between the pressure difference (ΔP) between the interior and exterior of the injector and the volumetric flow rate that regulates emptying time (Figure 3c). To the first order, this pressure depends on the force applied by the actuator and the area of the base of the injector, and it is responsible for creating the pressure difference that prompts flow. As the designed injector loading volume is 8.6 μL, and a suitable emptying time is ∼1 s, a minimum desirable volumetric flow rate is approximately 10 μL·s^{-1} as denoted by the purple line in Figure 3c. The actuator applies up to 250 mN supplementary pressure; thus, the actuator could apply up to ∼111 kPa to the 2.25 mm^2 base area. Critically, Figure 3c shows that rapid injection is achievable even at low channel diameters and pressures, e.g., 60 μm and 25 kPa, respectively. A channel diameter of 200 μm was chosen to ensure success of rapid delivery, wherein pressures of ≪25 kPa are expected to achieve successful injection. Notably, the backpressure in the intestinal tissue will inevitably result in a lower effective pressure differential; thus, the true injector pressure required for effective injection will likely be slightly higher than calculations performed here suggested. Nevertheless, this rapid and convective injection is expected to improve device reliability by mitigating misalignment caused by postactuation capsule movement. Moreover, the convective flow is expected to generate potential improvements to absorption by augmenting diffusion of drug molecules and vehicles toward absorptive tissues. Variation of channel geometry is expected to change the flow velocity and possibly the magnitude of this effect. Further analysis of these effects on transport in

https://doi.org/10.1021/acsami.5c05183
ACS Appl. Mater. Interfaces 2025, 17, 36420−36432

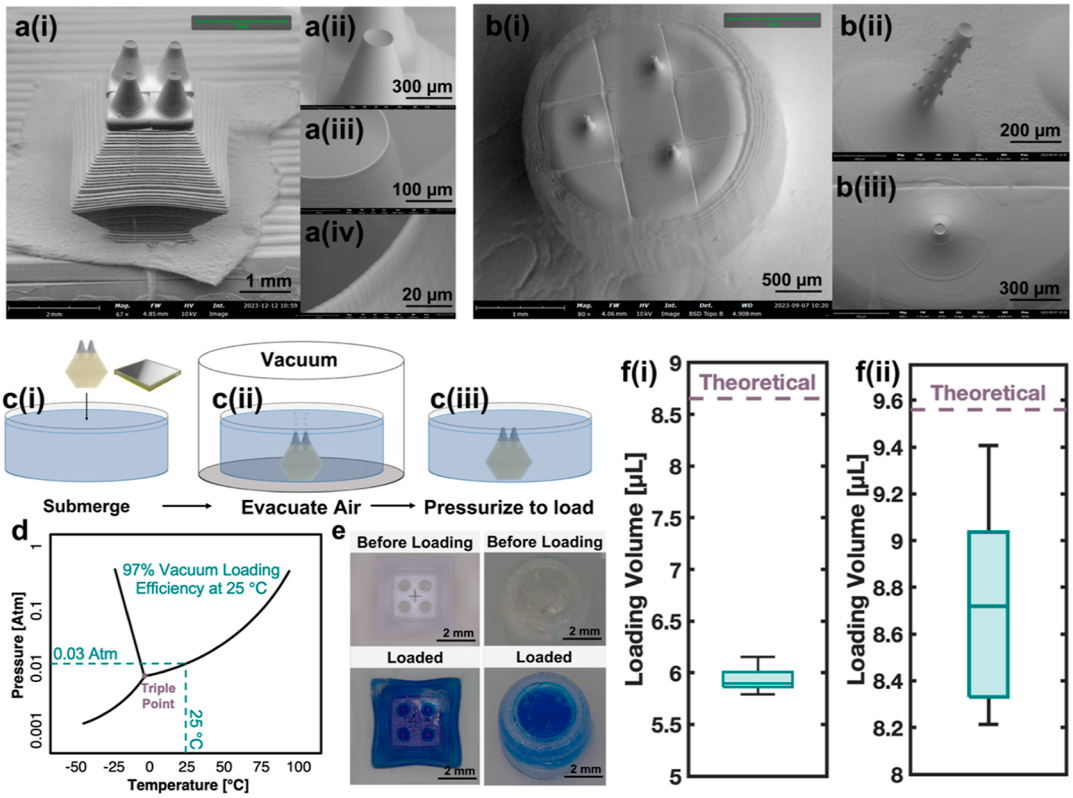

Figure 4. Injector structure and loading efficiency. (a) Scanning electron micrograph of the flexible injector highlighting the (a(i)) full injector and associated morphological structure, (a(ii)) conical microneedles, (a(iii)) surface of the microneedles, and (a(iv)) sharp tip of the microneedles achieved by the DLW process. (b) Scanning electron micrographs of the rigid injector highlighting the (b(i)) full injector and associated morphological structure and (b(ii)) barbed microneedles with the (b(iii)) hollow channel and sharp tip to control penetration and delivery rate. (c) Loading process of the injectors composed of (c(i)) submerging the injector in drug fluid, (c(ii)) evacuating the air using ∼95% vacuum, and (c(iii)) pressurization to load the drug into the injector. (d) The phase diagram of water shows the limitation of loading efficiency restricted by the vaporization of water in vacuum. (e) Before and after loading of the model drug into the rigid and flexible injectors. (f) The loading volume of the (f(i)) rigid injector and (f(ii)) flexible injector. Error bars represent standard deviation.

biological structures could unveil a new approach to control and improve drug absorption in the GI tract.

Computational Assessment of Rigid Injectors. While rapid injection is useful for enhanced reliability and bioavailability, targeted treatment of local disease sites can benefit from prolonged localized drug release, facilitating sustained treatment for more effective remediation of the disease. Injectors that rely predominantly on diffusion for drug release offer another modality of delivery that permits control of the delivery lifetime. Therefore, the developed diffusional injection technology is composed of a rigid reservoir and microneedles with three hollow channels for the regulation of drug release. The channel geometry can be used to adjust the rate of diffusion from within the injectors, where longer needles with smaller channel diameters are expected to restrict diffusion, leading to longer delivery lifetimes. To evaluate this effect, diffusion through various channel geometries was evaluated by using COMSOL Multiphysics software. A body of high concentration, representing the injector reservoir, was connected to an infinite low-concentration body, representing the intestinal tissue, via diffusion channels, and concentration inside the reservoir was computed throughout time (Figure 3d). The diffusion coefficient of a common corticosteroid for GI disease treatment, prednisone ($D = 0.728 \times 10^{-9}$ m^2 s^{-1}), was used as a representation of typical drug diffusion coefficients.[53] Channel diameters of 20 to 100 μm with channel lengths of 250 μm, 500 μm, and 750 μm were evaluated. For the purposes of comparison of the delivery lifetime, the delivery half-life was calculated from each data set. Figure 3e shows the resultant half-lives of various channel geometries. As anticipated, the larger channel diameters with shorter length resulted in more rapid delivery. Moreover, the number of needles could be used as another parameter to fine-tune the release rate of the drug from the injector. This model serves as a guide for design of injectors with targeted delivery lifetime for any drug species with a known diffusion coefficient.

Structural Properties of Injectors. The morphological properties of the injector are enabled by the hybrid fabrication approach and play a key role in the injector performance. Injectors were inspected via scanning electron microscopy to understand the interface robustness and structural features. Figure 4a(i) shows the flexible injector body and the attached conical hollow microneedles. The micrograph highlights the stair-like structure resulting from the 50 μm layer-by-layer VPP fabrication approach. This fabrication approach affords the ability to straightforwardly increase the size of the injector body to increase loading capacity with little addition to print time. The robust interface created by the 50 μm DLW interface overlap between the injector body and microneedles can be seen. Figure 4a(ii)−(iv) shows the rigid conical microneedles and resultant surface morphology using the DLW process. The ∼1 μm needle tip size and smooth surface enables effective penetration of the intestinal tissues with low required force while mitigating tissue damage. These proper-

https://doi.org/10.1021/acsami.5c05183
ACS Appl. Mater. Interfaces 2025, 17, 36420−36432

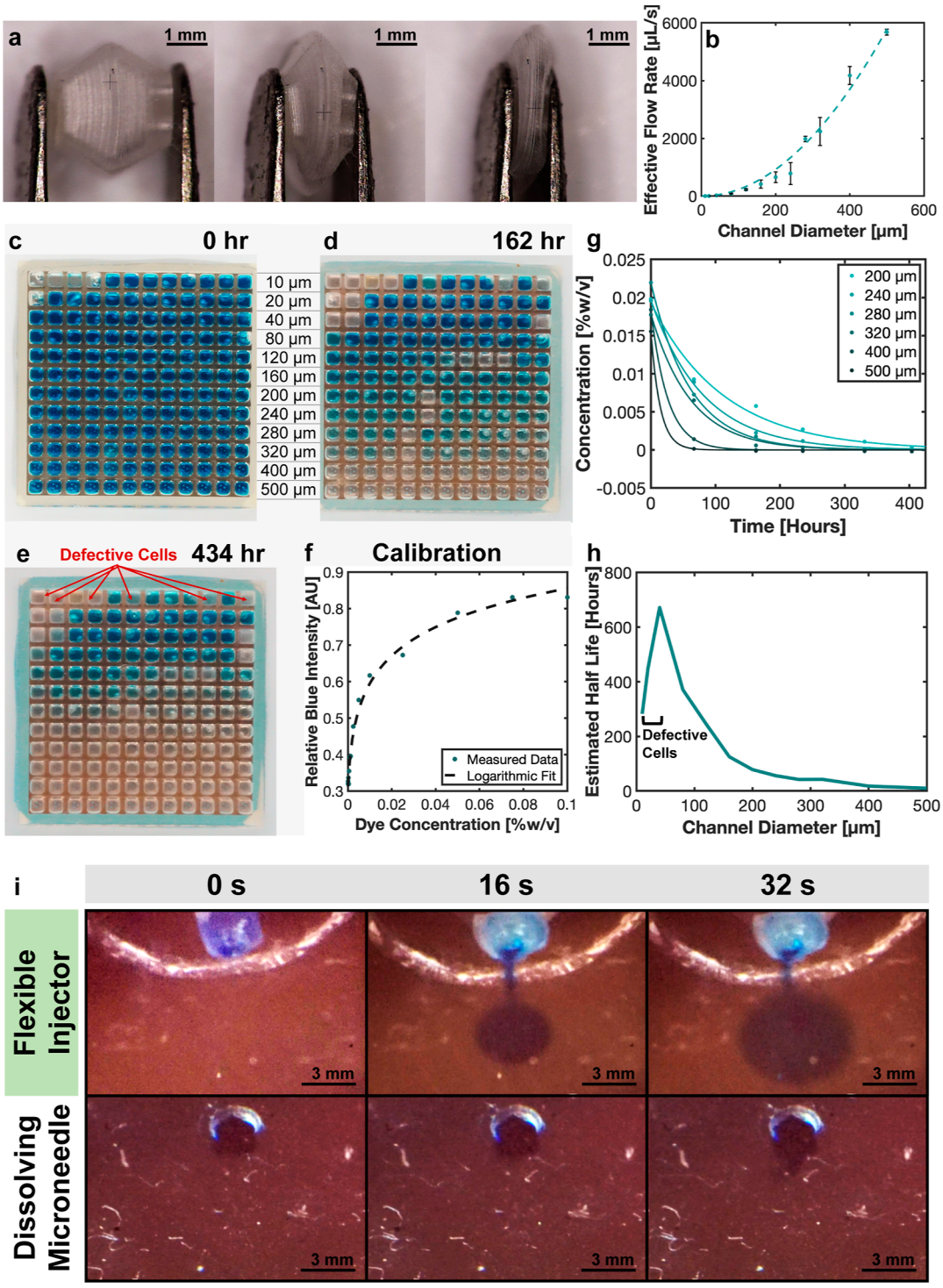

Figure 5. Evaluation of the flexible and rigid injectors. (a) Compression of the injector reservoir demonstrates material compliance without rupture. (b) The effective flow rate through flexible injectors for various channel sizes. (c–e) Images showing the back side of the diffusion array used to evaluate the rate of diffusion throughout 434 h. (f) The calibration curve used to assess the concentration inside the diffusion wells throughout due release. (g) Diffusion profiles from various injection channel diameters (n = 3). (h) Estimated diffusion half-life determined from diffusion data for 500 μm channel length. (i) Evaluation of the flexible injector by comparison with standard dissolving microneedles. The flexible injector shows both more rapid delivery time and improved convective transport compared to the dissolving needles.

ties, coupled with the tailored rigidity of the injector, enable the flexible injector microneedles to insert into the intestinal tissue before injector compression commences.

Figure 4b shows the rigid injector body with attached barbed microneedles. The rigid injector mirrors the stair-like surface and robust interface adhesion seen on the flexible injector. However, while the flexible injector utilizes rapid injection, the rigid injector is left behind in the intestinal tissue and thus must remain anchored to diffusively release the drug over time. Biomimetic anchoring barbs first presented in our lab by Liu et al. are utilized to enforce robust anchoring in intestinal tissue.[54−56] The anchoring microneedles that mimic a spiny-

https://doi.org/10.1021/acsami.5c05183
ACS Appl. Mater. Interfaces 2025, 17, 36420−36432

headed worm proboscis, a parasite that anchors in intestinal tissue, have demonstrated a high pull-out to penetration force ratio (PPR) of over 100. The blend of meso-to-micro scale features enabled by the hybrid approach facilitated such intricate strategies to enhance device performance. Moreover, the approach is amenable to rapid prototyping and design modification to enable additional functions such as directional release or features to mitigate tissue entrance in the needles.

Loading of Microneedle Injectors. The injectors are loaded using a vacuum loading process, as detailed in Figure 4c. The injectors are placed in the drug fluid, then air is evacuated from the reservoir by vacuum, followed by pressurization to force the drug fluid to enter the reservoir through the channels in the injector. Commonly, drugs are dissolved or suspended in water, which limits the ability of the solution to endure high or ultrahigh vacuum due to the vaporization pressure of the water solvent. Given the phase diagram of water (Figure 4d), the maximum achievable loading efficiency is expected to be approximately 97%. Due to the small channel and reservoir sizes, a notable characteristic of the injectors is their ability to retain the liquid in the injector before delivery via surface forces. This retention allows for transport and use without inadvertent drug loss. Moreover, the vacuum loading process is well-suited for large-scale manufacturing as vacuum processing is widely used across a variety of manufacturing industries. The loading efficiencies of both rigid and flexible injectors were characterized using dye release spectrophotometry experiments. The injectors before and after loading of 0.1% w/v FD&C Blue #1 dye solution are shown in Figure 4e. After loading, ultrasonically assisted release of the dye into a known volume of DI water was performed, and spectrophotometry was used to determine the final solution concentration. Using the initial concentration, final concentration, and final volume, the initial volume inside the reservoir was determined (n = 6) for each injector type. Figure 4f(i) shows the loading volume of the flexible injector (5.93 ± 0.13 μL), and Figure 4f(ii) shows the loading volume of the rigid injector (8.74 ± 0.43 μL).

The flexible injector loading volume was 31.4% lower than the design volume, and the rigid injector loading volume was 8.6% lower than the design volume. The deviation can be attributed to three error sources of varying degrees. First, the loading volume will be reduced due to the inability to achieve ultrahigh vacuum during the loading process. Second, dimensional inaccuracies are expected due to the slight shrinkage of photopolymers during the curing process. Finally, in the case of the flexible reservoir, the compliance of the reservoir body allows it to deform slightly when perturbed, possibly reducing the capacity. While the microliter volumes demonstrated here are expected to be effective for localized delivery of many drugs, the variable loading volume using this approach is a distinct advantage of this hybrid approach, supporting tailoring of the loading volume by changing reservoir geometry. The demonstrated loading process assumes that the drug constituents can undergo partial vacuum; however, there may be cases where sensitive constituents may not support vacuum loading. In this case, an alternative approach to introducing drugs into the reservoir can be used. One option is the use of vacuum preloading of the solvent, followed by diffusional loading of the drugs when submerged in a drug solution. Moreover, the use of constituents that are stable in water is important with this approach. Powder loading of the reservoirs is an alternate method for drugs that are unstable in water; however, the effectiveness of release control using the injectors with powdered drugs has yet to be evaluated.

Rapid Delivery via the Flexible Injector. A key characteristic to ensure proper operation of the flexible injector is the injection rate. In theoretical models, the injector showed the capacity to inject rapidly with channel diameters as small as 60 μm and pressures as low as 25 kPa. The flexible injector was evaluated using a simulated injection array to understand the injection rate for a variety of channel sizes at 35 kPa. Laser-drilled channels in 750 μm thick 304 stainless steel injection arrays were used to evaluate channel flow. The channel array was attached to a custom 3D-printed array flow array to facilitate the attachment of pressurized water to the channels. A 35 kPa water pressure source was attached to the array, and the volumetric flow rate through each channel size was evaluated. The effective flow rate was calculated as shown in Calculation S3 to account for the flow resistance in the test apparatus. Figure 5b shows the effective flow rate for various channel diameters (n = 3). Flow rate followed a consistent trend, increasing with larger channel size, as shown in Figure 5b. When compared to the prior injector flow models, comparable flow rates were achieved at smaller channel diameters; however, larger channels exhibited slower flow than predicted by the model. The reason for this could arise from systematic errors like flow inefficiencies or insufficient correction for test apparatus flow resistance. Nevertheless, the flow rates achievable here demonstrate the clear feasibility of rapidly injecting in under 1 s. As the reservoir volume is ∼6 μL, flow rates of 10 μL·s^{-1} will readily achieve rapid injection. Channel diameters of 40 μm and above showed the capacity to achieve this goal under the 35 kPa applied pressure.

To assess the ability of the fabricated injector to inject into a simulated environment and evaluate the convective flow postinjection, dye was injected into a DI water bath using a custom test apparatus. Force was applied to the back side of the injector by using a 30.5 g mass to approximate a 300 mN actuator force achieved in prior actuation capsules. Figure 5i shows the injection of the dye solution into the water at various time points. A traditional dissolving microneedle array is used as a comparison to benchmark both the delivery rate and postinjection transport in the simulated environment. The injector delivers the full payload within approximately 1 s after the weight is placed on the back of the injector, achieving the targeted delivery time frame to mitigate failures resulting from motion in the intestinal tract. In the following 13 s, the model drug fluid transports through the water until reaching the edge of the container, then begins to spread laterally. When compared to the dissolving microneedles, the injector prompts significantly faster injection with enhanced transport. The dissolving microneedles appear stagnant and release over >5 days, necessitating a form of anchoring in the intestinal tissue. Further demonstration of model drug delivery from the capsule actuator can be seen in Figure S7, where the device was deployed in ex vivo intestinal tissue. Evidenced by the rapid injection in both cases, the flexible injector obviates the need for anchoring, moreover, enhancing transport in the intestinal tissue and potentially enabling greater absorption of drugs in the tissue.

Prolonged Delivery via Diffusional Injection. To evaluate the diffusion rate through various channel sizes, a custom test apparatus was created to recapitulate the diffusion conditions from the rigid injector. The test apparatus is

https://doi.org/10.1021/acsami.5c05183
ACS Appl. Mater. Interfaces 2025, 17, 36420−36432

composed of an array of trichannel diffusion wells and enables repeated analysis across a variety of channel sizes between 20 and 500 μm in diameter as shown in Figure S8. The diffusion arrays are created by first laser-drilling the channels into a 750 μm 304 stainless steel plate, then mounting the plate on custom-fabricated 3D-printed diffusion wells created to replicate the drug reservoir. Diffusion arrays are vacuum loaded with a dye solution and placed in a water bath starting at $t = 0$. The dye concentration inside the diffusion well was determined via the relative color intensity inside the diffusion well, as defined in Calculation S1.

Figure 5f shows the calibration used to correlate the relative color intensity to the concentration in the reservoir ($n = 3$). Figure 5c–e shows the diffusion wells throughout the process of dye release into the surrounding water. From top to bottom of the image, the diffusion channels enlarge, as evidenced by the faster release of dye from the lower channels. The profiles of dye release through the channels of varying channel diameter are represented in Figure 5g ($n = 3$). Figure 5h presents the half-life of diffusion from within channels of varying diameter. Notably, the diffusion rate through channels of 10 and 20 μm exhibited uncharacteristic diffusion rates due to defects in the diffusion wells. These channel sizes are very small and require very long diffusion time frames, meaning that they may be less useful in practice than the larger channel sizes. The 40 μm diameter diffusion channel set showed an estimated half-life of 672 h, an approximate 4 week time frame until half of the dye was released. Larger channel diameters of 200 and 500 μm showed release half-lives of 78 and 10 h, respectively. The diffusion of the model drug from the injector into water is further evaluated in Figure S6, corroborating the results obtained using the diffusional test apparatus. The channel sizes demonstrated here show the effectiveness of the channel sizes for controlling diffusion rates from these injectors in a simulated system. When comparing the data acquired for 80 μm channels through simulation to the diffusion half-lives demonstrated here, the benchtop diffusion resulted in 2.83× slower diffusion. This difference can be partly attributed to the difference in diffusion coefficient between prednisone ($D = 0.728 \times 10^{-9}$ m^2·s^{-1}) and the FD&C Blue #1 ($D = 5.1 \times 10^{-9}$ m^2·s^{-1}) in water, balanced by the potential for convective currents to accelerate transport in the benchtop case.[57] The in vivo drug release rates are expected to deviate from the performed benchtop experiments given the difference in the diffusional and convective environment. Investigation of the comparative delivery rate in future in vivo evaluations is expected to provide a basis for calibrating benchtop data. Nevertheless, the controlled benchtop experiments will provide a framework to interpret changes in delivery rates based on the GI environment and diffusion coefficient of the species to be delivered.

The diffusional mode of delivery is an appealing approach because it allows controlled delivery profiles but also offers future potential for enhanced control methods. For example, the use of dynamic channel geometries with dissolving or swelling materials could allow sustained delivery with a linear release profile, and the use of external perturbants, such as ultrasound, could allow on-command release at times of need. Overall, the long-term performance of the rigid injector could be transformative for the delivery of corticosteroid drugs like budesonide or immune modulating agents like azathioprine that are commonly delivered as a daily oral dose and can cause significant side effects.[58] The sustained localized dosing from the rapid injector could significantly improve the treatment efficacy while reducing side effects.

While the technology has shown the ability to directly control the rate of drug release for prolonged delivery, a key challenge is achieving temporary device retention for the full duration of drug delivery. The anchoring barbs effectively attach to the intestinal tissue as reported previously; however, attachment to the intestinal epithelium is expected to last only approximately 3–7 days due to the cellular turnover and shedding. Needles designed to reach the lamina propria and muscularis are expected to permit longer residency times, depending also on the extent of immune response.[59−61] In the small intestine, these physiological structures exist at varying depths in the tissue. For example, the epithelium resides at the surface of the tissue and is only ∼10 μm deep, while the lamina propria sits behind the epithelium with a depth of 200–500 μm.[62,63] To target attachment to these structures, needles can be deliberately designed with lengths that reach the target tissue type. Moreover, this depth-tailoring approach nicely complements the relationship between the diffusion channel length and delivery half-life, where longer channels are well-suited for prolonged drug delivery. Following release from the intestinal tissue, the injectors are expected to be expelled from the body following passage through the large intestine within 12–72 h.[64] Future research in vivo will address this question by evaluating the relationship between the microneedle length and residency time. The biocompatibility of the injectors will play a large role in residency time and safety, as the foreign body immune response would likely prompt quicker expulsion of the injector from the body. However, the materials used for injector fabrication, including the reservoirs and needles, are all ISO 10993-5 biocompatible. Importantly, prior research evaluated the biocompatibility of the IP-Q material used to fabricate the needles, concluding no statistically significant impact on cell viability.[65] Moreover, prior experiments using the biomimetic barbed microneedles and other larger microneedles have been performed on porcine intestinal tissue without inducing significant tissue damage or perforation.[28,54,55,66,67] While the GI tract is a highly resilient environment and not expected to experience lasting damage from the microscale needles, the future investigation of the impacts of needle properties on residency time will yield insights into the immune response and tissue adaptation during residency.

Versatility of Delivery Species. The work here demonstrates the operation of the injectors with molecular constituents dissolved in water; however, certain drug types and applications require varied formulations to achieve therapeutic efficacy. The size, hydrophobicity, and solvent type required for each drug type will play a large role in determining the usefulness of each injector. The most critical parameter that determines injector suitability is the diffusion coefficient. Most water-soluble drug species will be compatible with the rigid injector because they can be dissolved in molecular form in water. Due to the molecular nature, the size and diffusion coefficient of these species are generally high ($>10^{-10}$ m^2·s^{-1}) compared to nanomaterials like liposomes, lipid nanoparticles, and polymeric nanoparticles that often have diffusion coefficients $\ll 10^{-10}$ m^2·s^{-1}.[68] Low diffusion rates may necessitate the use of the flexible injector, as the diffusional injector may not permit drug release in a suitable time frame. Figure S3 shows a computational assessment of diffusion of polymeric nanoparticles ($D = 3 \times 10^{-12}$ m^2·s^{-1})

https://doi.org/10.1021/acsami.5c05183
ACS Appl. Mater. Interfaces 2025, 17, 36420−36432

from the rigid injector. Due to the low diffusion coefficient, injectors with the largest channels of Ø = 500 μm with a 250 μm length exhibited a high half-life of ∼30 days. This extended diffusion, coupled with potential issues of nanomaterial agglomeration, highlights the usefulness of the flexible injector for this application.

Other applications of drug delivery may require the use of solvents other than water. In some cases, lipophilic drugs are dissolved in organic oils or in suspensions. These cases will reduce or eliminate the usefulness of diffusion, requiring a flexible injector. Finally, the use of injectors for ethanol ablation of fistulae is another promising use case in which the use of flexible or rigid injectors may provide distinct efficacy advantages. The viscosity of these different fluids will play a role in the performance of both the flexible and rigid injectors. Higher viscosity fluids will cause slower loading and pumping of the flexible injector and slower diffusion from the rigid injector. However, these modifications are expected to be predictable and not hinder the ability of the device to perform effectively in the GI environment. In fact, higher viscosity liquids will have the benefit of being more resilient to inadvertent leakage of the drug from the injectors. Future in vitro and in vivo evaluations of therapeutic delivery from the injectors will yield insight into the performance in combination with each constituent type. Overall, the versatility of design, scale, and performance achievable using flexible and rigid injectors unlocks a wealth of opportunities for exploration of drug types and delivery approaches.

CONCLUSION

This work demonstrates development of a drug delivery technology for local drug injection in the GI tract that enables an unprecedented level of control over the delivery half-life. The injection technology is composed of two key elements: an LCD-printed body with variable material properties to control compression and a microneedle array fabricated using a versatile DLW approach to leverage microneedle geometry for control of injection rate and location. This work demonstrates both a rigid injector that relies on diffusion for prolonged delivery and a flexible injector that delivers rapidly. FEM modeling and benchtop evaluation showed loading volumes of >5 μL and injection half-lives between 4 s and 118 days, providing excellent versatility. Moreover, the system is a demonstration of the capacity of hybrid fabrication approaches to solve challenges of multiscale construction. Overall, the injection system paired with previously developed ingestible capsule technologies would enable enhanced control over localized drug delivery in the GI tract.

EXPERIMENTAL METHODS

3D Printing of Rigid and Flexible Reservoirs. Injector reservoirs were designed using Autodesk Fusion 360 (San Francisco, CA, USA). The rigid reservoir has an outer diameter of 3 mm, a 200 μm wall thickness, and three 400 μm holes at a radial distance of 600 μm and separated 120° radially from the center on the reservoir top surface for drug passage. A custom base was designed to insert into the Nanoscribe Photonic Professional GT+ sample holder. The base consists of a 25 × 25 × 2 mm plate, and the reservoirs are designed on 2 mm tall pedestals attaching to the plate in a 3 × 3 reservoir array spaced by 4 mm on the center. Stereolithography files were sliced by using the CHITUBOX slicer program (Shenzen, CN). Reservoirs are fabricated via liquid-crystal display (LCD) vat photopolymerization (VPP) 3D printing using the Phrozen Sonic Mini 8K 3D printer (Hsinchu City, Taiwan). To fabricate rigid reservoirs, FormLabs Surgical Guide v2 biocompatible (ISO 10993-5 and 10993-10 compliant) photoresin is used with a 50 μm layer thickness and 3.5 s of layer exposure time. To fabricate flexible injectors, 3Dresyns Bioflex A50 MB biocompatible flexible resin (A50 hardness; ISO 10993-5 compliant) with a 50 μm layer height and 7 s layer exposure time is used. Following removal from the printer build plate, parts are cleaned via an ultrasonic isopropanol bath for 5 min, then repeating 3 times. Reservoirs are then posted in the Phrozen UV Cure Station for 45 min.

Direct Laser Writing of Attached Microneedles. Hollow microneedles are printed directly on the reservoirs using the Nanoscribe Photonic Professional GT+ (Karlsruhe, DE) with the 10× LF Print Set as previously described by Sarker et al.[69] Microneedles were designed using Autodesk Fusion 360. Barbed microneedles for the rigid injector have a wall thickness of 15 μm, a height of 750 μm, and 24 anchoring barbs with a 13 μm base diameter and 20 μm length. Conical hollow microneedles for the flexible injector have a channel size of 200 μm with a 750 μm height and 600 μm base diameter. Stereolithography files for the microneedle designs were sliced using the DeScribe software with a 3 μm slicing distance, 50 mW laser power, and 100,000 $\mu m \cdot s^{-1}$ scan speed. Nanoscribe IP-Q photoresin was first vacuum loaded into the injector reservoir, and then a drop of the IP-Q was placed on top of the reservoir for printing. The reservoir/IP-Q interface was found manually, and the print was started 50 μm below the top surface of the injector to ensure proper adhesion. Following printing, the injector array was developed using a 2 h propylene glycol methyl ether acetate (PGMEA) bath cycled through vacuum to ensure fluid exchange between the interior and exterior of the reservoir. Injectors were dried and detached from their pedestals before loading.

Loading of Model Drugs. Drugs are loaded into the injector using the vacuum loading process shown in Figure 4c. Injectors are first submerged in the model drug solution, a 0.1% w/v solution of FD&C Blue #1 dye. The submerged injectors are placed in a vacuum chamber and brought from atmospheric pressure to ∼0.05 atm at a rate of ∼0.05 atm/min. After evacuation of air from the reservoirs, the chamber is returned to atmospheric pressure at ∼0.05 atm/min. Following the loading process, the injectors were applied to the previously demonstrated actuator capsule using the process shown in Figure S4.

The loading volume of the injectors was evaluated by evaluating solution concentration after simulated delivery. Following loading of the FD&C Blue #1, individual rigid (n = 6) and flexible (n = 6) reservoirs were placed in tubes of 10 mL DI water. Tubes underwent ultrasonic exposure for 1 h using the Branson M1800 ultrasonic bath (Brookfield, CT, USA) to promote rapid transport of the dye from inside the reservoirs. Once dissolved in the 10 mL solution, a sample of the solution was evaluated using the Molecular Devices SpectraMax Plus 384 Spectrophotometer (San Jose, CA, USA) to obtain the absorbance. The absorbance was correlated to a predetermined calibration curve (Figure S5) for FD&C Blue #1 dye to obtain the final concentration. With the known final volume, final concentration, and initial concentration, the initial drug volume inside the reservoir was calculated.

Modeling of Injector Diffusion. Diffusion from injectors was modeled in COMSOL Multiphysics 5.4 (Burlington, MA, USA) using the diffusion of dilute species module. A cylindrical domain (Ø = 2.4 mm and height = 2 mm) was arranged with three cylindrical channels of variable diameter and length leading to a reservoir. The concentration inside the reservoir was measured throughout time for a variety of channel lengths and diameters of 250−750 and 20−100 μm, respectively. The diffusion coefficient of prednisone (D = 0.728×10^{-9} $m^2 \cdot s^{-1}$) in water, a common corticosteroid for GI treatment, was used as a representation of dissolved drug species. Additional evaluation of diffusion of larger species, such as drug nanocarriers, was approximated with $D = 3 \times 10^{-12}$ $m^2 \cdot s^{-1}$.[68] The diffusion half-life was determined as described in Calculation S2.

Modeling of Injector Compression. Compression of the flexible injector was assessed using the COMSOL Multiphysics 5.4 (Burlington, MA, USA) structural mechanics module. The flexible

https://doi.org/10.1021/acsami.5c05183
ACS Appl. Mater. Interfaces 2025, 17, 36420−36432

reservoir geometry was imported from the Fusion 360 design file, and a fixed constraint was applied to the bottom surface of the injector. Force was applied to the top surface and displacement was measured. Structural constants were derived from the manufacturer-stated mechanical properties of the 3Dresyns Bioflex A50 MB Resin. The Young's modulus was calculated from the A50 hardness and established a relationship between Shore A hardness and modulus.[70] MATLAB was used to assess flow from inside the injector at various diameters and pressure differences using the Hagen−Poiseuille equation (Calculation S3). The dynamic viscosity of water at 25 °C (8.9×10^{-4} Pa·s) and a channel length of 750 μm were used.[71]

Injector Microscopy. Injectors were imaged using a Fischer Scientific Phenom XL scanning electron microscope (SEM). Samples were mounted to a specimen by using adhesive carbon tape. Low-vacuum scanning electron microscopy (LV-SEM) at 60 Pa with an acceleration voltage of 10 kV was used to mitigate the charging of the polymeric surfaces on the injector.

Fabrication of Diffusion Evaluation Apparatus. A custom-designed apparatus was fabricated to perform large-scale analysis of simulated diffusion from reservoirs. An array of square diffusion wells with a size of 3 × 3 mm and 1 mm spacing was fabricated via LCD 3D printing using the Phrozen Sonic Mini 8K with FormLabs Surgical Guide v2 resin with a layer height of 50 μm and a cure time of 3.5 s followed by the same cleaning and postcuring process used for the injector reservoirs. Laser-drilled 304 stainless steel diffusion plates were purchased from JEM Lasers (Milpitas, CA, USA) in arrangements parallel to the patterns of rigid and flexible injector needle spacing and geometry. For each three-channel set, the channels are separated 120° radially at a distance of 600 μm from the center. The diffusion plates have a 12 × 12 array of channel sets separated by 4 mm on the center to align with the well array. Well arrays were sealed on one side by placement of the array in a Petri dish filled to a 200 μm layer of FormLabs Surgical Guide V2 photoresin and then UV-cured for 45 min. Diffusion plates were then adhered to the well array using FormLabs Surgical Guide V2 photoresin and UV-cured for an additional 45 min.

Evaluation of Diffusional Injection. FD&C Blue #1 dye dissolved in DI water was loaded into the reservoir array using the vacuum loading process presented in Figure 3c. Imaged color intensity was used to quantify the dye concentration in the wells throughout time. A calibration curve was established to understand the relationship between the relative blue intensity and dye concentrations between 0.001 and 0.1% w/v. Following calibration, a ∼0.02% w/v dye solution was loaded into the diffusion array and the array was placed in a water bath. Diffusion was tracked via imaging of the array backside, using the calibration equation to determine the concentration in each cell and time point (n = 3).

Assessment of Forced Injection. The forced injection of drug solution was evaluated using laser-drilled 304 stainless steel plates and via injection into a fluid bath. 304 stainless steel plates with a thickness of 750 μm were purchased from JEM Lasers (Milpitas, CA, USA). Plates contain laser-drilled channels with diameters of 10−500 μm arranged in 2 × 2 arrays comparable to the arrangement of needles on the flexible injector with 750 μm x−y spacing. The arrays are arranged in a 12 × 12 pattern with 4 mm interspacing on the center. A 3D-printed array of 3 × 3 mm large flow channels are attached to the flow plate to allow connection of a pressurized water line. The flow rate through each channel diameter was measured (n = 3) by determining the time required to fill a specified volume at 35 kPa. The volumetric flow rate was corrected for the internal flow resistance of the water supply, and the rates were compared for channels of varying diameter (Calculation S3).

Flexible injectors were tested by injection of FD&C Blue #1 dye solution into a water bath and compared to dissolving microneedles. A square hole (1 mm × 1 mm) was created in a 254 μm polyethylene terephthalate (PET) film as a support to enable compression and visualization of injection from the injector. The PET film was thermally bonded to a Ø = 100 mm Petri dish and filled with DI water. The injector was placed on the square hole in the PET film and a 30.5 g mass was applied to the back of the reservoir to approximate an ingestible actuator force. Injection of FD&C Blue #1 was filmed during compression. Placement of dissolving poly(vinyl alcohol) (PVA) microneedles in the square hole was used to compare performance to current molded microneedle technologies. PVA microneedles were fabricated by solution casting of dye-embedded PVA solution as presented by Levy et al.[67]

■ ASSOCIATED CONTENT

Supporting Information

The Supporting Information is available free of charge at https://pubs.acs.org/doi/10.1021/acsami.5c05183.

Design and dimensioning of flexible and rigid injectors; computational evaluation of nanoparticle diffusion; injector assembly on the actuator; calibration of dye in water; diffusion from a rigid injector; deployment of injectors from the actuator capsule; design of delivery test plates; calculation of dye concentration from color intensity; processing of diffusion data; and evaluation of corrected flow through injectors (PDF)

■ AUTHOR INFORMATION

Corresponding Author

Reza Ghodssi − *Department of Materials Science and Engineering, University of Maryland, College Park, Maryland 20742, United States; The MATRIX Lab, Robert E. Fischell Institute for Biomedical Devices, Fischell Department of Bioengineering, and Department of Electrical and Computer Engineering, University of Maryland, College Park, Maryland 20742, United States;* orcid.org/0000-0002-3716-4901; Email: ghodssi@umd.edu

Authors

Joshua A. Levy − *Department of Materials Science and Engineering, University of Maryland, College Park, Maryland 20742, United States; The MATRIX Lab and Robert E. Fischell Institute for Biomedical Devices, University of Maryland, College Park, Maryland 20742, United States;* orcid.org/0000-0002-9567-5822

Michael A. Straker − *The MATRIX Lab, Robert E. Fischell Institute for Biomedical Devices, and Fischell Department of Bioengineering, University of Maryland, College Park, Maryland 20742, United States*

Justin M. Stine − *The MATRIX Lab, University of Maryland, College Park, Maryland 20742, United States*

Jude A. C. Stephen − *Department of Electrical and Computer Engineering, University of Maryland, College Park, Maryland 20742, United States*

Complete contact information is available at: https://pubs.acs.org/10.1021/acsami.5c05183

Author Contributions

J.A.L., M.A.S., and R.G. were responsible for the conceptualization of the research concepts. J.A.L. and M.A.S. were responsible for the research methodology. J.A.L. and J.A.C.S. were responsible for investigation into diffusion from injectors. J.A.L., J.A.C.S., and J.M.S. visualized data and images for the manuscript. J.M.S. and R.G. provided supervisory support for the research. J.A.L. and M.A.S. were responsible for drafting the manuscript. J.A.L., M.A.S., J.M.S., and R.G. were responsible for reviewing and editing the manuscript.

Funding

The authors acknowledge support by the U.S. National Science Foundation (NSF) ECCS program under award #1939236.

Notes

The authors declare no competing financial interest.

■ ACKNOWLEDGMENTS

The authors acknowledge support from the Clark Doctoral Fellows Program, TerrapinWorks, the University of Maryland Nanocenter and its FABLAB.

■ REFERENCES

(1) Alqahtani, M. S.; Kazi, M.; Alsenaidy, M. A.; Ahmad, M. Z. Advances in Oral Drug Delivery. *Front. Pharmacol* **2021**, *12*, 62.
(2) Kim, J.; De Jesus, O. *Medication Routes of Administration*; StatPearls, 2022.
(3) Greenwood-Van Meerveld, B.; Johnson, A. C.; Grundy, D. Gastrointestinal Physiology and Function. *Handb. Exp. Pharmacol.* **2017**, *239*, 1.
(4) Chu, J. N.; Traverso, G. Foundations of Gastrointestinal-Based Drug Delivery and Future Developments. *Nat. Rev. Gastroenterol. Hepatol.* **2022**, *19* (4), 219−238.
(5) Luo, Z.; Paunović, N.; Leroux, J. C. Physical Methods for Enhancing Drug Absorption from the Gastrointestinal Tract. *Adv. Drug Delivery Rev.* **2021**, *175*, 113814.
(6) Volk, N.; Lacy, B. Anatomy and Physiology of the Small Bowel. *Gastrointest. Endosc. Clin. N. Am.* **2017**, *27* (1), 1−13.
(7) Ensign, L. M.; Cone, R.; Hanes, J. Oral Drug Delivery with Polymeric Nanoparticles: The Gastrointestinal Mucus Barriers. *Adv. Drug Delivery Rev.* **2012**, *64* (6), 557.
(8) Bandi, S. P.; Bhatnagar, S.; Venuganti, V. V. K. Advanced Materials for Drug Delivery across Mucosal Barriers. *Acta Biomater.* **2021**, *119*, 13−29.
(9) Rowland, M. Influence of Route of Administration on Drug Availability. *J. Pharm. Sci.* **1972**, *61* (1), 70−74.
(10) Vinarov, Z.; Abdallah, M.; Agundez, J. A. G.; Allegaert, K.; Basit, A. W.; Braeckmans, M.; Ceulemans, J.; Corsetti, M.; Griffin, B. T.; Grimm, M.; Keszthelyi, D.; Koziolek, M.; Madla, C. M.; Matthys, C.; McCoubrey, L. E.; Mitra, A.; Reppas, C.; Stappaerts, J.; Steenackers, N.; Trevaskis, N. L.; Vanuytsel, T.; Vertzoni, M.; Weitschies, W.; Wilson, C.; Augustijns, P. Impact of Gastrointestinal Tract Variability on Oral Drug Absorption and Pharmacokinetics: An UNGAP Review. *Eur. J. Pharm. Sci.* **2021**, *162*, 105812.
(11) Hua, S. Advances in Oral Drug Delivery for Regional Targeting in the Gastrointestinal Tract - Influence of Physiological, Pathophysiological and Pharmaceutical Factors. *Front. Pharmacol* **2020**, *11*, 524.
(12) Gavhane, Y. N.; Yadav, A. V. Loss of Orally Administered Drugs in GI Tract. *Saudi Pharm. J.* **2012**, *20* (4), 331.
(13) Ghosh, A.; Li, L.; Xu, L.; Dash, R. P.; Gupta, N.; Lam, J.; Jin, Q.; Akshintala, V.; Pahapale, G.; Liu, W.; Sarkar, A.; Rais, R.; Gracias, D. H.; Selaru, F. M. Gastrointestinal-Resident, Shape-Changing Microdevices Extend Drug Release in Vivo. *Sci. Adv.* **2020**, *6* (44), 4133−4161.
(14) Schoellhammer, C. M.; Schroeder, A.; Maa, R.; Lauwers, G. Y.; Swiston, A.; Zervas, M.; Barman, R.; DiCiccio, A. M.; Brugge, W. R.; Anderson, D. G.; Blankschtein, D.; Langer, R.; Traverso, G. Ultrasound-Mediated Gastrointestinal Drug Delivery. *Sci. Transl. Med.* **2015**, *7* (310), 310ra168.
(15) Byrne, J.; Huang, H. W.; McRae, J. C.; Babaee, S.; Soltani, A.; Becker, S. L.; Traverso, G. Devices for Drug Delivery in the Gastrointestinal Tract: A Review of Systems Physically Interacting with the Mucosa for Enhanced Delivery. *Adv. Drug Delivery Rev.* **2021**, *177*, 113926.
(16) Xia, D.; Wood-Yang, A. J.; Prausnitz, M. R. Clearing Away Barriers to Oral Drug Delivery. *Sci. Robot.* **2022**, *7* (70), No. eade3311.
(17) Date, A. A.; Hanes, J.; Ensign, L. M. Nanoparticles for Oral Delivery: Design, Evaluation and State-of-the-Art. *J. Controlled Release* **2016**, *240*, 504.
(18) Laffleur, F.; Bernkop-Schnürch, A. Strategies for Improving Mucosal Drug Delivery. *Nanomedicine* **2013**, *8* (12), 2061−2075.
(19) Zierden, H. C.; Josyula, A.; Shapiro, R. L.; Hsueh, H. T.; Hanes, J.; Ensign, L. M. Avoiding a Sticky Situation: Bypassing the Mucus Barrier for Improved Local Drug Delivery. *Trends Mol. Med.* **2021**, *27* (5), 436−450.
(20) Wang, L.; Liu, Q.; Hu, X.; Zhou, C.; Ma, Y.; Wang, X.; Tang, Y.; Chen, K.; Wang, X.; Liu, Y. Enhanced Oral Absorption and Liver Distribution of Polymeric Nanoparticles through Traveling the Enterohepatic Circulation Pathways of Bile Acid. *ACS Appl. Mater. Interfaces* **2022**, *14* (37), 41712−41725.
(21) Lu, X.; Li, J.; Xue, M.; Wang, M.; Guo, R.; Wang, B.; Zhang, H. Net-Neutral Nanoparticles-Extruded Microcapsules for Oral Delivery of Insulin. *ACS Appl. Mater. Interfaces* **2023**, *15* (28), 33491−33503.
(22) Li, Q.; Liu, W.; Liu, K.; Dong, Z.; Kong, W.; Lu, X.; Wei, Y.; Wu, W.; Yang, J.; Qi, J. The Role of Nanoparticle Morphology on Enhancing Delivery of Budesonide for Treatment of Inflammatory Bowel Disease. *ACS Appl. Mater. Interfaces* **2024**, *16* (26), 33081−33092.
(23) Reinholz, J.; Landfester, K.; Mailänder, V. The Challenges of Oral Drug Delivery via Nanocarriers. *Drug Delivery* **2018**, *25* (1), 1694.
(24) Chehelgerdi, M.; Chehelgerdi, M.; Allela, O. Q. B.; Pecho, R. D. C.; Jayasankar, N.; Rao, D. P.; Thamaraikani, T.; Vasanthan, M.; Viktor, P.; Lakshmaiya, N.; Saadh, M. J.; Amajd, A.; Abo-Zaid, M. A.; Castillo-Acobo, R. Y.; Ismail, A. H.; Amin, A. H.; Akhavan-Sigari, R. Progressing Nanotechnology to Improve Targeted Cancer Treatment: Overcoming Hurdles in Its Clinical Implementation. *Mol. Cancer* **2023**, *22* (1), 169.
(25) Huang, H.; Lyu, Y.; Nan, K. Soft Robot-Enabled Controlled Release of Oral Drug Formulations. *Soft Matter* **2023**, *19* (7), 1269−1281.
(26) Schoellhammer, C. M.; Traverso, G. Low-Frequency Ultrasound for Drug Delivery in the Gastrointestinal Tract. *Expert Opin. Drug Delivery* **2016**, *13* (8), 1045.
(27) Chen, W.; Wainer, J.; Ryoo, S. W.; Qi, X.; Chang, R.; Li, J.; Lee, S. H.; Min, S.; Wentworth, A.; Collins, J. E.; Tamang, S.; Ishida, K.; Hayward, A.; Langer, R.; Traverso, G. Dynamic Omnidirectional Adhesive Microneedle System for Oral Macromolecular Drug Delivery. *Sci. Adv.* **2022**, *8* (1), 1792.
(28) Abramson, A.; Caffarel-Salvador, E.; Soares, V.; Minahan, D.; Tian, R. Y.; Lu, X.; Dellal, D.; Gao, Y.; Kim, S.; Wainer, J.; Collins, J.; Tamang, S.; Hayward, A.; Yoshitake, T.; Lee, H. C.; Fujimoto, J.; Fels, J.; Frederiksen, M. R.; Rahbek, U.; Roxhed, N.; Langer, R.; Traverso, G. A Luminal Unfolding Microneedle Injector for Oral Delivery of Macromolecules. *Nat. Med.* **2019**, *25* (10), 1512−1518.
(29) Abramson, A.; Caffarel-Salvador, E.; Khang, M.; Dellal, D.; Silverstein, D.; Gao, Y.; Frederiksen, M. R.; Vegge, A.; Hubálek, F.; Water, J. J.; Friderichsen, A. V.; Fels, J.; Kirk, R. K.; Cleveland, C.; Collins, J.; Tamang, S.; Hayward, A.; Landh, T.; Buckley, S. T.; Roxhed, N.; Rahbek, U.; Langer, R.; Traverso, G. An Ingestible Self-Orienting System for Oral Delivery of Macromolecules. *Science* **2019**, *363* (6427), 611−615.
(30) Traverso, G.; Schoellhammer, C. M.; Schroeder, A.; Maa, R.; Lauwers, G. Y.; Polat, B. E.; Anderson, D. G.; Blankschtein, D.; Langer, R. Microneedles for Drug Delivery via the Gastrointestinal Tract. *J. Pharm. Sci.* **2015**, *104* (2), 362.
(31) Gareb, B.; Otten, A. T.; Frijlink, H. W.; Dijkstra, G.; Kosterink, J. G. W. Review: Local Tumor Necrosis Factor-α Inhibition in Inflammatory Bowel Disease. *Pharmaceutics*. MDPI AG June 1, 2020; pp 1−31. DOI: .
(32) Eder, P.; Zielińska, A.; Karczewski, J.; Dobrowolska, A.; Słomski, R.; Souto, E. B. How Could Nanobiotechnology Improve Treatment Outcomes of Anti-TNF-α Therapy in Inflammatory Bowel Disease? Current Knowledge, Future Directions. *J. Nanobiotechnol.* **2021**, *19*, 346.
(33) Schultz, D.; Kempen, P. J.; Primdahl, S.; Pereverzina, M.; Uhrenfeldt, A. H.; Alba, E. M. D.; Andreasen, J.; Pedersen, H. D.; Cleveland, C.; Duncombe, T.; Ahnfelt-Rønne, J.; Kirk, R. K.; Pfander, I. B.; Sticker, D.; Water, J. J.; Buckley, S. T.; Andresen, T. L.; Urquhart, A. J. Gastrointestinal Device-Mediated Delivery of MRNA-

https://doi.org/10.1021/acsami.5c05183
ACS Appl. Mater. Interfaces 2025, 17, 36420−36432

Lipid Nanoparticles Achieves Distinct Expression and Biodistribution in Mice and Pigs. *ACS Appl. Mater. Interfaces* **2024**, *16*, 67192−67202.
(34) Widjaja, M.; Gan, J.; Talpaneni, J. S. R.; Tjandrawinata, R. R. Determination of Eudragit® L100 in an Enteric-Coated Tablet Formulation Using Size-Exclusion Chromatography with Charged-Aerosol Detection. *Sci. Pharm.* **2018**, *86* (3), 38.
(35) Hashim, M.; Korupolu, R.; Syed, B.; Horlen, K.; Beraki, S.; Karamchedu, P.; Dhalla, A. K.; Ruffy, R.; Imran, M. Jejunal Wall Delivery of Insulin via an Ingestible Capsule in Anesthetized Swine—A Pharmacokinetic and Pharmacodynamic Study. *Pharmacol. Res. Perspect.* **2019**, *7* (5), No. e00522.
(36) Ghorbani Siavashani, A.; Rehan, M.; Travas-Sejdic, J.; Thomas, D.; Diller, E.; Stine, J.; Ghodssi, R.; Avci, E. Ingestible Smart Capsules for Chemical Sensing in the Gut. *Anal. Chem.* **2025**, *97* (10), 5343−5354.
(37) Fox, C. B.; Cao, Y.; Nemeth, C. L.; Chirra, H. D.; Chevalier, R. W.; Xu, A. M.; Melosh, N. A.; Desai, T. A. Fabrication of Sealed Nanostraw Microdevices for Oral Drug Delivery. *ACS Nano* **2016**, *10* (6), 5873−5881.
(38) Van Der Schaar, P. J.; Dijksman, J. F.; Broekhuizen-De Gast, H.; Shimizu, J.; Van Lelyveld, N.; Zou, H.; Iordanov, V.; Wanke, C.; Siersema, P. D. A Novel Ingestible Electronic Drug Delivery and Monitoring Device. *Gastrointest. Endosc.* **2013**, *78* (3), 520−528.
(39) Yim, S.; Goyal, K.; Sitti, M. Magnetically Actuated Soft Capsule With the Multimodal Drug Release Function. *IEEE ASME Trans. Mechatron.* **2013**, *18* (4), 1413.
(40) Mapara, S. S.; Patravale, V. B. Medical Capsule Robots: A Renaissance for Diagnostics, Drug Delivery and Surgical Treatment. *J. Controlled Release* **2017**, *261*, 337−351.
(41) Cortegoso Valdivia, P.; Robertson, A. R.; De Boer, N. K. H.; Marlicz, W.; Koulaouzidis, A. An Overview of Robotic Capsules for Drug Delivery to the Gastrointestinal Tract. *J. Clin. Med.* **2021**, *10* (24), 5791.
(42) Pi, X.; Lin, Y.; Wei, K.; Liu, H.; Wang, G.; Zheng, X.; Wen, Z.; Li, D. A Novel Micro-Fabricated Thruster for Drug Release in Remote Controlled Capsule. *Sens. Actuators, A* **2010**, *159* (2), 227−232.
(43) Verma, M.; Vishwanath, K.; Eweje, F.; Roxhed, N.; Grant, T.; Castaneda, M.; Steiger, C.; Mazdiyasni, H.; Bensel, T.; Minahan, D.; Soares, V.; Salama, J. A. F.; Lopes, A.; Hess, K.; Cleveland, C.; Fulop, D. J.; Hayward, A.; Collins, J.; Tamang, S. M.; Hua, T.; Ikeanyi, C.; Zeidman, G.; Mule, E.; Boominathan, S.; Popova, E.; Miller, J. B.; Bellinger, A. M.; Collins, D.; Leibowitz, D.; Batra, S.; Ahuja, S.; Bajiya, M.; Batra, S.; Sarin, R.; Agarwal, U.; Khaparde, S. D.; Gupta, N. K.; Gupta, D.; Bhatnagar, A. K.; Chopra, K. K.; Sharma, N.; Khanna, A.; Chowdhury, J.; Stoner, R.; Slocum, A. H.; Cima, M. J.; Furin, J.; Langer, R.; Traverso, G. A Gastric Resident Drug Delivery System for Prolonged Gram-Level Dosing of Tuberculosis Treatment. *Sci. Transl. Med.* **2019**, *11* (483), 6267.
(44) Xitian, P.; Hongying, L.; Kang, W.; Yulin, L.; Xiaolin, Z.; Zhiyu, W. A Novel Remote Controlled Capsule for Site-Specific Drug Delivery in Human GI Tract. *Int. J. Pharm.* **2009**, *382* (1−2), 160−164.
(45) Park, J.; Bertsch, A.; Martin-Olmos, C.; Brugger, J. Nanoliter Liquid Packaging in a Bioresorbable Microsystem by Additive Manufacturing and Its Application as a Controlled Drug Delivery Device. *Adv. Funct. Mater.* **2023**, *33* (38), 2302385.
(46) Dietzel, C. T.; Richert, H.; Abert, S.; Merkel, U.; Hippius, M.; Stallmach, A. Magnetic Active Agent Release System (MAARS): Evaluation of a New Way for a Reproducible, Externally Controlled Drug Release into the Small Intestine. *J. Controlled Release* **2012**, *161* (3), 722−727.
(47) Becker, D.; Zhang, J.; Heimbach, T.; Penland, R. C.; Wanke, C.; Shimizu, J.; Kulmatycki, K. Novel Orally Swallowable IntelliCap®Device to Quantify Regional Drug Absorption in Human GI Tract Using Diltiazem as Model Drug. *Ageing Int.* **2014**, *15* (6), 1490−1497.
(48) Lee, J.; Lee, H.; KwonPark, S. S. . h.; Park, S. Active Delivery of Multi-Layer Drug-Loaded Microneedle Patches Using Magnetically Driven Capsule. *Med. Eng. Phys.* **2020**, *85*, 87−96.
(49) Lee, J.; Kim, D.; Bang, S.; Park, S. Drug-Loaded Mucoadhesive Patch with Active Delivery and Controlled Releasing Ability. *Adv. Intell. Syst.* **2022**, *4* (4), 2100203.
(50) Levy, J. A.; Straker, M. A.; Stine, J. M.; Beardslee, L. A.; Ghodssi, R. Magnetically Triggered Ingestible Capsule for Localized Microneedle Drug Delivery. *Device* **2024**, *2* (10), 100438.
(51) Stone, H. A.; Stroock, A. D.; Ajdari, A. Engineering Flows in Small Devices: Microfluidics toward a Lab-on-a-Chip. *Annu. Rev. Fluid. Mech.* **2004**, *36*, 381−411.
(52) Tarbox, T. N.; Watts, A. B.; Cui, Z.; Williams, R. O. An Update on Coating/Manufacturing Techniques of Microneedles. *Drug Delivery Transl. Res.* **2018**, *8* (6), 1828−1843.
(53) Seki, T.; Mochida, J.; Okamoto, M.; Hosoya, O.; Juni, K.; Morimoto, K. Measurement of Diffusion Coefficients of Parabens and Steroids in Water and 1-Octanol. *Chem. Pharm. Bull.* **2003**, *51* (6), 734−736.
(54) Liu, S.; Chu, S.; Beardslee, L. A.; Ghodssi, R. Hybrid and Passive Tissue-Anchoring Mechanism for Ingestible Resident Devices. *J. Microelectromech. Syst.* **2020**, *29* (5), 706.
(55) Liu, S.; Chu, S.; Banis, G. E.; Beardslee, L. A.; Ghodssi, R. Biomimetic Barbed Microneedles for Highly Robust Tissue Anchoring. *Proceedings of the IEEE International Conference on Micro Electro Mechanical Systems (MEMS)* 2020, IEEE 2020-January, 885−888, .
(56) Levy, J. A.; Straker, M. A.; Stine, J. M.; Beardslee, L. A.; Borbash, V.; Ghodssi, R. Thermomechanical Soft Actuator for Targeted Delivery of Anchoring Drug Deposits to the GI Tract. *Adv. Mater. Technol.* **2023**, *8* (2), 2201365.
(57) Gimadutdinova, L.; Ziyatdinova, G.; Davletshin, R. Selective Voltammetric Sensor for the Simultaneous Quantification of Tartrazine and Brilliant Blue FCF. *Sensors* **2023**, *23* (3), 1094.
(58) Crohns & Colitis Foundation. Fact Sheet: News from the IBD Help Center. https://www.crohnscolitisfoundation.org/sites/default/files/legacy/assets/pdfs/immunomodulators.pdf (accessed Dec 15 2024).
(59) Veisman, I.; Massey, W. J.; Goren, I.; Liu, W.; Chauhan, G.; Rieder, F. Muscular Hyperplasia in Crohn's Disease Strictures: Through Thick and Thin. *Am. J. Physiol. Cell Physiol.* **2024**, *327* (3), C671−C683.
(60) Arike, L.; Seiman, A.; van der Post, S.; Rodriguez Piñeiro, A. M.; Ermund, A.; Schütte, A.; Bäckhed, F.; Johansson, M. E. V.; Hansson, G. C. Protein Turnover in Epithelial Cells and Mucus along the Gastrointestinal Tract Is Coordinated by the Spatial Location and Microbiota. *Cell Rep.* **2020**, *30* (4), 1077−1087e3.
(61) Carnicer-Lombarte, A.; Chen, S. T.; Malliaras, G. G.; Barone, D. G. Foreign Body Reaction to Implanted Biomaterials and Its Impact in Nerve Neuroprosthetics. *Front. Bioeng. Biotechnol.* **2021**, *9*, 622524.
(62) Salva, M. N.; Gupta, C.; Pandey, A. K.; Kumar, N.; Kotian, S. R.; Kalthur, S. G. Histogenesis and Histomorphometric Study of Human Fetal Small Intestine. *Ethiop J. Health Sci.* **2019**, *29* (6), 689−696.
(63) Atuma, C.; Strugala, V.; Allen, A.; Holm, L. The Adherent Gastrointestinal Mucus Gel Layer: Thickness and Physical State in Vivo. *Am. J. Physiol. Gastrointest. Liver Physiol.* **2001**, *280* (5), G922−G929.
(64) Lee, Y. Y.; Erdogan, A.; Rao, S. S. C. How to Assess Regional and Whole Gut Transit Time With Wireless Motility Capsule. *J. Neurogastroenterol Motil* **2014**, *20* (2), 265.
(65) Isaakidou, A.; Apachitei, I.; Fratila-Apachitei, L. E.; Zadpoor, A. A. High-Precision 3D Printing of Microporous Cochlear Implants for Personalized Local Drug Delivery. *Journal of Functional Biomaterials* **2023**, *14* (10), 494.
(66) Abramson, A.; Dellal, D.; Kong, Y. L.; Zhou, J.; Gao, Y.; Collins, J.; Tamang, S.; Wainer, J.; McManus, R.; Hayward, A.; Frederiksen, M. R.; Water, J. J.; Jensen, B.; Roxhed, N.; Langer, R.;

Traverso, G. Ingestible Transiently Anchoring Electronics for Microstimulation and Conductive Signaling. *Sci. Adv.* **2020**, *6*, No. eaaz0127.
(67) Levy, J. A.; Straker, M. A.; Stine, J. M.; Beardslee, L. A.; Borbash, V.; Ghodssi, R. Thermomechanical Soft Actuator for Targeted Delivery of Anchoring Drug Deposits to the GI Tract. *Adv. Mater. Technol.* **2023**, *8* (2), 2201365.
(68) Ramirez, A.; Merwitz, B.; Lee, H.; Vaughan, E.; Maisel, K. Multiple Particle Tracking (MPT) Using PEGylated Nanoparticles Reveals Heterogeneity within Murine Lymph Nodes and between Lymph Nodes at Different Locations. *Biomater. Sci.* **2022**, *10* (24), 6992.
(69) Sarker, S.; Colton, A.; Wen, Z.; Xu, X.; Erdi, M.; Jones, A.; Kofinas, P.; Tubaldi, E.; Walczak, P.; Janowski, M.; Liang, Y.; Sochol, R. D. 3D-Printed Microinjection Needle Arrays via a Hybrid DLP-Direct Laser Writing Strategy. *Adv. Mater. Technol.* **2023**, *8* (5), 2201641.
(70) Gent, A. N. On the Relation between Indentation Hardness and Young's Modulus. *Rubber Chem. Technol.* **1958**, *31* (4), 896−906.
(71) *CRC Handbook of Chemistry and Physics*, 52nd ed.; R, C. W., Ed.; Chemical Rubber: Cleveland, 1971.

https://doi.org/10.1021/acsami.5c05183
ACS Appl. Mater. Interfaces 2025, 17, 36420−36432